Laser-Driven Coherent Betatron Oscillation in a Laser-Wakefield Cavity

Károly Németh,[1,2,*] Baifei Shen,[1,2,3] Yuelin Li,[1,2] Hairong Shang,[1,2] Robert Crowell,[4] Katherine C. Harkay,[1,2] and John R. Cary[5,6]

[1]*Accelerator Systems Division, Argonne National Laboratory, Argonne, Illinois 60439, USA*
[2]*Argonne Accelerator Institute, Argonne National Laboratory, Argonne, Illinois 60439, USA*
[3]*State Key Laboratory of High Field Laser Physics, Shanghai Institute of Optics and Fine Mechanics, P.O. Box 800-211, Shanghai 201800, China*
[4]*Chemistry Division, Argonne National Laboratory, Argonne, Illinois 60439, USA*
[5]*Center for Integrated Plasma Studies and Department of Physics, University of Colorado, Boulder, Colorado 80309, USA*
[6]*Tech-X Corporation, Boulder, Colorado 80303, USA*

(Received 20 April 2007; published 4 March 2008)

The origin of beam disparity in emittance and betatron oscillation orbits, in and out of the polarization plane of the drive laser of laser-plasma accelerators, is explained in terms of betatron oscillations driven by the laser field. As trapped electrons accelerate, they move forward and interact with the laser pulse. For the bubble regime, a simple model is presented to describe this interaction in terms of a harmonic oscillator with a driving force from the laser and a restoring force from the plasma wake field. The resulting beam oscillations in the polarization plane, with period approximately the wavelength of the driving laser, increase emittance in that plane and cause microbunching of the beam. These effects are observed directly in 3D particle-in-cell simulations.

DOI: 10.1103/PhysRevLett.100.095002 PACS numbers: 52.38.Kd, 41.75.Ht, 41.75.Jv

Laser-wakefield acceleration (LWFA) [1,2] has produced narrow-spread, GeV electron beams [3–6] from centimeters of laser-plasma interaction, thus demonstrating acceleration gradients of order of 50 GeV/m, 3 orders of magnitude greater than in conventional accelerators. To improve reproducibility and reliability, laser injection has been proposed [7–10], self-consistently simulated [9,11], and observed experimentally [12]. Commonly observed is transverse asymmetry of the beam, including the betatron amplitude in Ref. [13] and the asymmetric beam profile in Ref. [14]. This asymmetry leads to increased emittance of the beam in the polarization plane. Microbunching of the beam is also described in Ref. [15]. Lack of rotational symmetry of beams has also been observed in simulations [16] of beams in the *bubble regime* [3].

In this Letter, we show that the asymmetry of the beam originates from its direct interaction with the laser, which occurs as the beam accelerates and moves forward in the bubble. A simple model shows how this interaction causes transverse oscillations in the plane of polarization, ultimately leading to larger emittance in that plane. Three-dimensional particle-in-cell (PIC) simulations show the details of this process. The beam is seen to acquire a significant oscillation, as shown in Fig. 1, that is a fair fraction of the extent of the bubble. This process also leads to microstructure of the beam. Our results indicate that the emittance disparity is an intrinsic property of bubble-regime acceleration.

Betatron oscillations are fundamental to the dynamics in accelerators [17]. They lead to synchrotron radiation, which has been observed in experiments for both laser-driven plasmas [18] or beam driven plasmas [19], and has been used for imaging the betatron trajectories of electrons in plasma [13]. In conventional accelerators, betatron motion can be driven by focusing magnets along the beam line. Resonantly driven coherent betatron oscillations by

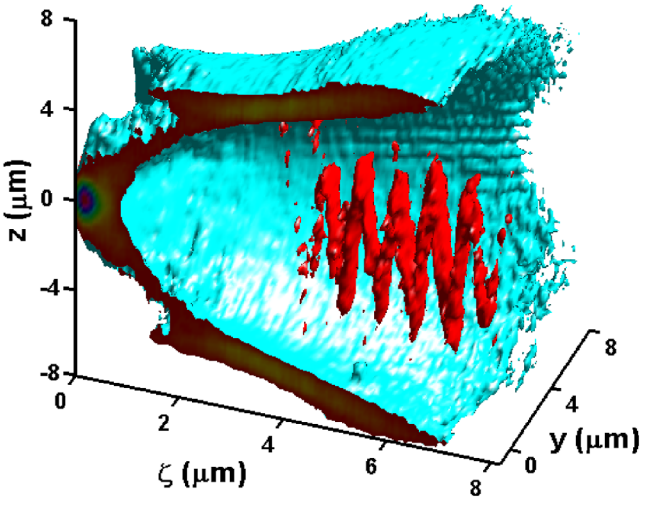

FIG. 1 (color online). Electron density distribution at $t = 6.2$ ps from 3D PIC simulations showing the structure of the bubble and the accelerated beam. The sinusoid structure of the beam is a result of the laser-driven coherent betatron oscillation. Note that the laser propagates in the x direction, and it is linearly polarized in the z direction. ζ denotes the distance from the base of the bubble along x. The volumes of the injected electrons are indicated by electron isodensity surfaces of $6.2 \times 10^{19} 1/\mathrm{cm}^3$ and the volumes of the shell of the bubble by isodensity surfaces of $1.86 \times 10^{20} 1/\mathrm{cm}^3$.

transversely oscillating magnetic fields have also been observed [20].

Because of the laser-driven betatron oscillation, the beam can obtain a highly regular sinusoidal structure in the polarization plane of the laser (see Fig. 1), while it remains tightly confined in the perpendicular plane. The wavelength of the sinusoidal structure approximately equals the wavelength of the local laser field. We show that this coherent betatron oscillation provides an explanation of the observed beam asymmetries and microbunching mentioned above.

Our computations of this phenomenon were carried out using the VORPAL [21] computational framework, which computes the evolution of charged particles and fluids in the presence of electromagnetic fields and collisional effects. We present the results for parameters similar to those of the laser-injection experiments by Faure *et al.* [12]. The driving pulse had a laser strength (normalized vector potential) of $a_+ = 1.3$, a slightly elliptical focal spot of 16×21 μm (with the shorter diameter in the polarization direction) and a duration of 30 fs (peak power $\approx$14 *TW*). The injection pulse had a strength of $a_- = 0.4$, a circular focal spot of 31 μm diameter and a 30 fs duration. All geometric or duration parameters are given in full width at half maximum (FWHM). Both pulses were Gaussian with a wavelength of $\lambda_L = 820$ nm and linear polarization in the z direction, while propagating along the x axis. The 3D simulation box was 48 μm in the x direction and 60 μm in the transverse directions. The grid contained 20 points per laser (plasma) wavelength in the longitudinal (transverse) directions, respectively. Each cell contained two macroparticles ($\approx$56 436 electrons). A moving window algorithm was used. Driving and injection pulses were focused to the injection point, x_{inj}, with location determined from the middle of the plasma. The plasma density was 7.5×10^{18} cm^{-3} with a 1.5 mm plateau between 0.4 mm ramps.

A "bubble" is a 3D plasma wave formed when the electrons are pushed away by an intense laser pulse, leaving a cavity behind. Electrons flow on the surface of the bubble and collide at its base, where they may get injected and trapped into the bubble due to large enough local electric field or appropriate electron energy distribution caused, e.g., by the injecting laser pulse. The injected electrons are accelerated by the bubble's electric field [3]. Figure 1 shows the plasma density distribution for $x_{\text{inj}} = -30$ μm case, when the electron beam reaches the middle of the bubble, at $t = 6.2$ ps, with $t = 0$ being the time the driving pulse enters the plasma and $t = 3.94$ ps the time when the two laser pulses collide. The beam has a regular sinusoid shape in the polarization (xz) plane of the laser, with an amplitude of 2.5–5.0 μm, while it is confined in the perpendicular direction with a uniform thickness of <1 μm. The period of the sinusoid structure changes from about 660 nm (right after injection, at $t =$ 4.6 ps) to about 800 nm (before the beam leaves the plasma, at $t = 7.7$ ps)—approximately the same as the wavelength of the laser.

The scaling of the beam oscillations with laser wavelength is confirmed by 2D PIC simulations with drive-laser wavelengths varying from 820 to 300 nm and laser strengths of $a_+ = 2.3$ and $a_- = 0.4$. This is shown in Fig. 2, which gives the variation of the amplitude and wavelength of the beam oscillation with time for lasers of two different wavelengths. This figure shows that the initial amplitude of the sinusoid decreases with the drive-laser wavelength. Because of a Doppler shift, the injected electron observes redshifted light at $2\gamma\lambda_L$, with γ being the electron's Lorentz factor; i.e., it spends more time in one light period. This allows more time for the development of transverse motions due to the laser force, and, as a consequence, the amplitude of the electron trajectory may become larger than λ_L and can further increase as the beam is accelerated.

The observations agree with the test-particle trajectory calculations described below. Comparing the frequency of the laser force, $k_x\xi/t$ (see definitions below) along the calculated trajectory to the betatron frequency ω_B at each moment of the propagation indicates that these frequencies are closer to resonance in the $\lambda_L = 820$ nm case than in the 300 nm one, thus high amplitude can be expected sooner for the $\lambda_L = 820$ nm case and later for the 300 nm case.

A simple model to calculate test-electron trajectories in the bubble supports this picture. The electric field in the bubble cavity is modeled by the electric field of a positively

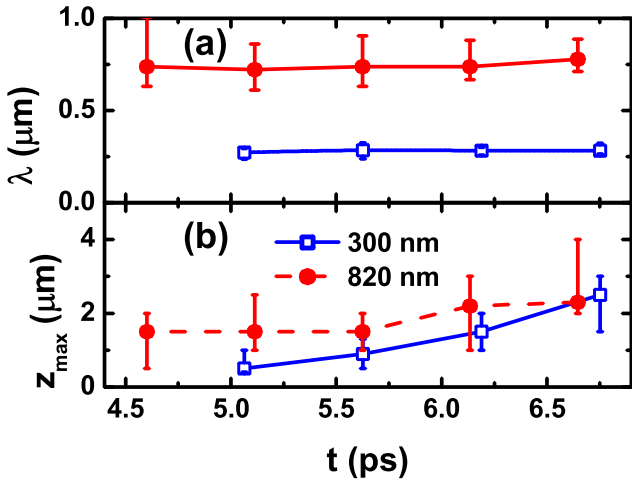

FIG. 2 (color online). Time-evolution (a) of the period λ of the beam structure and (b) that of the maximum beam amplitude (z_{max}) for laser wavelengths of $\lambda_L = 820$ and 300 nm in 2D PIC simulations for similar conditions as in Fig. 1. The beam structure, $z(x)$ has been defined by density-weighted z averages at every x, at each given time-point. The predominant peak in the Fourier transform of $z(x)$ determines λ. Error bars of z_{max} are visual estimates of the half-width of the beam. Error bars of the period, λ, are calculated from the FWHMs of the peaks of the Fourier tranforms of $z(x)$.

charged sphere with homogeneous charge distribution, similar to those described in Refs. [22,23]. The cavity follows the propagation of the laser pulse along the x direction at a distance equivalent to the radius of the bubble R, with a velocity equal to the group velocity of the laser pulse, V_g. Test electrons are injected at the base of the bubble, i.e., $2R$ behind the center of the laser pulse, along x. Thus, for the longitudinal acceleration, the equation of motion is

$$\frac{d}{dt}(\gamma m_e \dot{x}) = q_e[K(x - x_c) - \dot{z}B_y], \tag{1}$$

while for the transverse motion it is

$$\frac{d}{dt}(\gamma m_e \dot{z}) = q_e[Kz + E_z + \dot{x}B_y]; \tag{2}$$

E_z and B_y refer to the primary components of the electric and magnetic fields of the laser pulse. The gradient of the electric field due to the bubble is $K = m_e\omega_P^2/(3|q_e|) = 4.545 \times 10^{16}$ V/m^2 [22] (ω_P is the plasma-frequency). The center of the bubble is at $x_c = (R + V_g t)$. From the PIC simulations, $R = 6$ μm, half the plasma-wavelength [2,3].

The E_z electric and B_y magnetic fields of the laser pulse were set from the vector potential

$$A_z = A_L \cos[k_x x - \omega_L t], \tag{3}$$

with $A_L = A_0 \exp[-(x - (x_c + R))^2/\Delta X_L^2]$ as $E_z = -\partial A_z/\partial t$ and $B_y = -\partial A_z/\partial x$. $A_0 = E_0/(k_x V_p)$ with $E_0 = 2 \times 10^{12}$ V/m being the effective amplitude of the laser's E-field in the vicinity of the injected electrons as taken from the PIC calculations. ΔX_L is the pulse-duration, $\omega_L = 2\pi c/\lambda_L$, and $k_x = \omega_L/V_p$, with V_p the phase velocity of the laser.

The above expressions E_z and B_y allow Eq. (2) to be put into the form,

$$z'' + \frac{\gamma'}{\gamma}z' + \frac{2\omega_B^2}{\dot{\xi}^2}z = \frac{q_e A_L}{m_e \gamma \dot{\xi}}\left[k_x \sin(k_x \xi) + \frac{2(\xi - 2R)}{\Delta X_L^2}\left(1 + \frac{\Delta V}{\dot{\xi}}\right)\cos(k_x \xi)\right], \tag{4}$$

with $\omega_B^2 = -q_e K/2m_e\gamma$, $\Delta V = V_p - V_g$, and $\xi = x - V_p t$. $\zeta = x - V_g t$ measures the distance of the electron from the base of the bubble ($\zeta = \xi + \Delta V t$). Prime in the superscript denotes derivative by ξ. Equation (4) is analogous to a periodically driven harmonic oscillator [24] with a damping term of γ'/γ, a frequency of ω_B, and an oscillating driving force, on the right-hand side of Eq. (4), except that the damping term and the fundamental and driving frequencies are time dependent due to beam acceleration. This analogy to the classical oscillator suggests that, after a transitory period when oscillations due to the solution of the zero-driving case decline in time, the periodicity of the transverse oscillations will be determined solely by the driving force. Furthermore, the amplitude and phase of the resulting oscillation loses memory of the initial conditions. Thus, along ξ, the trajectory of the oscillation is

$$z \propto \sin(k_x \xi + \varphi), \tag{5}$$

where φ is the relative phase of the trajectory and the laser. By virtue of the analogy to classical mechanics we can expect that φ becomes approximately identical for each injected electron after the decline of transitory effects and leads to coherent electron trajectories along ξ. At a fixed t^* time, $z(x, t^*) \propto \sin(k_x x - k_x V_p t^* + \varphi)$, which means that the electrons of the beam are placed along a single sinusoid wave, just as observed in the PIC calculations. As $k_x = \omega_L/V_p$, coherence of the trajectories appears only at a V_p that equals with the factual phase velocity of the laser. This phase velocity has been found to be $V_p = 0.9985c$ from analysis of the time evolution of the laser field in the vicinity of the injected electrons. Analysis of the motion of the base of the bubble provides an effective $V_g = 0.9925c$.

The above analogy has been verified by numerically solving Eqs. (1) and (4) for the case in which ΔX_L is large, so that the envelope of the vector potential becomes constant, $A_L = A_0$. Initial ζ and z coordinates were randomly taken from $\zeta, z \in [-0.5, 0.5]$ μm, which represents the extent of the base. The magnitude of the initial velocity was calculated from a γ value randomly taken from $\gamma \in [\gamma_0, 2\gamma_0]$, with $\gamma_0 = 1/\sqrt{1 - (V_g/c)^2}$. The angle of initial velocity to the x axis was randomly chosen with the constraint of $\dot{x} \geq V_g$. The amplitude of the magnetic field obtained from the vector potential, 6.25 kT, has been readjusted to 7.25 kT to better reproduce the PIC data (5–10 kT) in the region of the injected electrons. Six thousand electrons have been injected, by 0.4 fs delays during a 2.5 ps period (full evolution period of PIC beam) and let propagate until reaching the middle of the bubble (8.75 ps with $t = 0$ for the first injection). The resulting beam structure is depicted in Fig. 3(b), and is compared to the PIC beam. The periodicity of both the trajectories and the beam is seen to be determined by the laser wavelength (Fig. 3). The longer time needed for the propagation of the test electrons is probably due to insufficient modelling of the injection circumstances. We did not refine our model further as we aimed only on the reproduction of the core features of the phenomenon, such as the periodicity and amplitude of the beam and the ξ dependence of the trajectories on the basis of a minimalistic model.

The propagation of the beam after leaving the plasma was calculated using the GPT code [25]. The beam is found to be microbunched due to the periodic transverse momentum distribution, as shown in Fig. 4. The bunching persists several cm after the plasma, and the beam diverges quickly in the polarization plane of the light. The emittance at

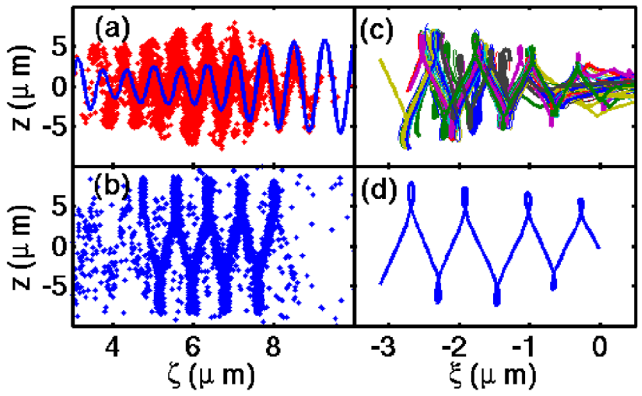

FIG. 3 (color online). Distribution of electrons from the PIC simulation (a) and from test electrons (b) in the xz plane and (a) that of the B_y field (along the x axis, scaled by 3×10^{-4} μm/T), at $t = 6.2$ ps, ζ is the distance from the base of the bubble. Note that the electrons move in phase with the B field of the laser. Trajectories of some of the highest energy electrons (c) and a test-electron one (d) show similar amplitudes and periodicity along $\xi = x - V_p t$, with $V_p = 0.9985c$.

4 mm is 1.5×10^{-6} m rad in the y direction and 88×10^{-6} m rad in z.

For a shorter drive pulse ΔX_L, the amplitude of the oscillation grew more slowly. This is also confirmed by 3D PIC simulations. Changing the duration of the drive pulse from 30 to 10 fs, while keeping all other parameters fixed, results in small (<1 μm), poorly defined oscillations in the xz plane until the beam gets close to the drive pulse in the second half of the bubble, where oscillations increase and become better defined. This indicates that pulse shaping, such that minimal laser field is present in the latter half of the bubble, where acceleration occurs, may minimize the large emittance in the plane of polarization. In the case of self trapping (no injection pulse) we also observe sinusoid structures, but less well defined, only after a longer time spent in overlap with the bulk of the pump pulse. This indicates the approximate validity of the driven oscillator model for these cases as well.

In conclusion, the observed [14] emittance disparity in and out of the plane of laser polarization in the bubble regime with laser injection [12] is explained as being the result of betatron oscillations driven directly by the laser field. The betatron oscillations (observed in [13]) are computed using a simple model that is found to be consistent with 3D PIC simulations. Thus, the amplitude and wavelength of these oscillations is predicted. Beam microbunching, observed in [15], is also explained. Finally, we indicate how pulse shaping might mitigate the formation of these oscillations and, thus, improve beam quality.

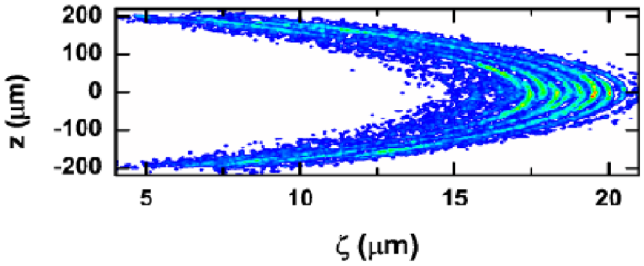

FIG. 4 (color online). Microbunching of the beam at 4 mm propagation after leaving the plasma.

Computational help and discussions with R. Soliday, K-J. Kim, A. Lumpkin, E. Frank, W. Gropp (Argonne), and D. Bruhwiler (Tech-X) are gratefully acknowledged. This research was supported by the U. S. DOE Office of Science, under Contracts No. DE-AC02-06CH11357, No. DE-FG02-01ER41178, No. DE-FC02-07ER41499, and No. DE-FG02-04ER41317. The authors thank NERSC (No. DE-AC02-05CH11231) for the use of computational resources. We also acknowledge the VORPAL team: G. I. Bell, D. L. Bruhwiler, R. S. Busby, J. Carlsson, J. R. Cary, D. A. Dimitrov, A. Hakim, P. Messmer, P. Mullowney, C. Nieter, K. Paul, S. W. Sides, N. D. Sizemore, D. N. Smithe, P. H. Stoltz, R. Trines, S. A. Veitzer, D. J. Wade-Stein, W.-L. Wang, G. R. Werner, N. Xiang.

*Nemeth@ANL.Gov

[1] T. Tajima and J. M. Dawson, Phys. Rev. Lett. **43**, 267 (1979).
[2] Eric Esarey *et al.*, IEEE Trans. Plasma Sci. **24**, 252 (1996).
[3] A. Pukhov *et al.*, Appl. Phys. B **74**, 355 (2002).
[4] S. P. D. Mangles *et al.*, Nature (London) **431**, 535 (2004).
[5] J. Faure *et al.*, Nature (London) **431**, 541 (2004).
[6] W. P. Leemans *et al.*, Nature Phys. **2**, 696 (2006).
[7] D. Umstadter *et al.*, Phys. Rev. Lett. **76**, 2073 (1996).
[8] E. Esarey *et al.*, Phys. Rev. Lett. **79**, 2682 (1997).
[9] J. R. Cary *et al.*, *Proc. Part. Accel. Conf.* p. 719 (2003), http://accelconf.web.cern.ch/AccelConf/.
[10] G. Fubiani *et al.*, Phys. Rev. E **70**, 016402 (2004).
[11] J. R. Cary *et al.*, Phys. Plasmas **12**, 056704 (2005).
[12] J. Faure *et al.*, Nature (London) **444**, 737 (2006).
[13] K. Ta Phuoc *et al.*, Phys. Rev. Lett. **97**, 225002 (2006).
[14] S. P. D. Mangles *et al.*, Phys. Rev. Lett. **96**, 215001 (2006).
[15] Y. Glinec *et al.*, Phys. Rev. Lett. **98**, 194801 (2007).
[16] F. S. Tsung *et al.*, Phys. Rev. Lett. **93**, 185002 (2004).
[17] For example, see S. Y. Lee, *Accelerator Physics* (World Scientific, Singapore, 1999).
[18] A. Rousse *et al.*, Phys. Rev. Lett. **93**, 135005 (2004).
[19] S. Wang *et al.*, Phys. Rev. Lett. **88**, 135004 (2002).
[20] M. Bai *et al.*, Phys. Rev. E **56**, 6002 (1997).
[21] C. Nieter and J. R. Cary, J. Comput. Phys. **196**, 448 (2004).
[22] A. Pukhov *et al.*, Plasma Phys. Controlled Fusion **46**, B179 (2004).
[23] W. Lu *et al.*, Phys. Rev. Lett. **96**, 165002 (2006).
[24] For example, see J. M. González-Miranda, *Synchronization and Control of Chaos* (Imperial College Press, London, 2004).
[25] S. B. van der Geer *et al.*, Inst. Phys. Conf. Ser. No. 175, 101 (2005).